# Light extraction in individual GaN nanowires on Si for LEDs

Jordan Chesin[a], Xiang Zhou[a] and Silvija Gradečak[a]
[a] Department of Materials Science and Engineering, Massachusetts Institute of Technology
77 Massachusetts Ave., Cambridge, MA 02139, USA.

## ABSTRACT

GaN-based nanowires hold great promise for solid state lighting applications because of their waveguiding properties and the ability to grow nonpolar GaN nanowire-based heterostructures, which could lead to increased light extraction and improved internal quantum efficiency, respectively. In addition, GaN nanowires can be grown directly on Si substrates, providing an inexpensive and scalable platform for device fabrication. We use finite difference time domain photonic simulations to explore light extraction efficiency enhancement in GaN nanowire-based light-emitting diodes (LEDs) on Si. Emission polarization and the placement of the emission source along the length of the nanowire were taken into consideration. We find that the optimal placement of the emission source is determined by the light reflection at the nanowire-air and nanowire-substrate interfaces and the coupling of emitted radiation into the waveguided modes, resulting in extraction efficiencies of up to 50%. Our approach to optimizing light extraction via simulation techniques can be applied to more realistic large-scale devices to guide experimental work towards nanowire-based LEDs with potentially greater efficiencies than their thin-film counterparts.

**Keywords:** light extraction, nanowires, LEDs, GaN, FDTD

## 1. INTRODUCTION

GaN is a wide bandgap semiconductor that has become the material of choice for the solid-state lighting industry[1]. There is great interest in GaN-based materials for white light-emitting diode (LED) applications due to the potential to tune light emission from $In_xGa_{1-x}N$ quantum wells (QWs) over a wide range of wavelengths via the composition of the alloy[2]. Controllable doping of both *n*-type and *p*-type GaN is now reliably achieved[3,4], making it suitable for a wide range of applications in optoelectronics, as well as for high-power, high-temperature electronics[5] and high electron mobility transistors[6,7]. Recently there has been much interest in integration of GaN on Si inspired by the potential for an inexpensive and scalable platform for growth[8,9], as opposed to sapphire ($Al_2O_3$) and SiC growth substrates. In addition to the cost and scalability, the Si platform also provides new device opportunities. For example, the use of a conductive substrate enables new LED configurations to ameliorate current crowding, which occurs in the mesa-structure often used for GaN-based LEDs[10,11]. However, whereas sapphire is transparent in the visible spectrum, Si absorbs and reflects most of the visible emission from LEDs[12] making some configurations, such as the flip-chip design[13], impractical. In addition, extended defects, such as dislocations, typically arise in GaN thin-films grown on lattice mismatched Si substrates and these can inhibit radiative recombination. Due to the high lattice mismatch and thermal expansion coefficient differences between GaN and Si, cracking of the film can occur upon cooling from growth temperatures[9] and large wafer curvatures can arise[14].

GaN nanowires, high aspect ratio materials that are typically less than a few hundred nanometers in width and many microns long, can address some of these materials challenges[15,16] and enable integration of GaN on Si[17]. The small nanowire-substrate interface over which lattice mismatch causes strain and the large nanowire surface area that relaxes the strain enables heteroepitaxy on largely mismatched substrates, while maintaining material of high structural quality, which is free of extended defects[18]. Nanowires also offer advantages in tuning structural and optical properties via the choice of metal seed-particle used in metal-organic chemical vapor deposition (MOCVD)[19]. The growth of nonpolar III-nitride nanowire heterostructures via MOCVD has recently been demonstrated[20] as a promising step towards axial nanowire-LEDs. QWs embedded in nanowires grown in the nonpolar *m*-direction ($\langle 1\bar{0}10 \rangle$), do not experience the quantum-confined Stark effect, characteristic for films and nanowires grown in the polar *c*-direction ($\langle 0001 \rangle$), and are therefore expected to have higher internal quantum efficiency (IQE) compared to devices based on heterostructures

Nanoepitaxy: Materials and Devices IV, edited by Nobuhiko P. Kobayashi, A. Alec Talin, M. Saif Islam,
Proc. of SPIE Vol. 8467, 846703 · © 2012 SPIE · CCC code: 0277-786/12/$18 · doi: 10.1117/12.970456

along polar directions[21]. Furthermore, GaN nanowires have the potential to increase extraction efficiency due to their waveguiding properties; depending on their diameter and structure, nanowires can guide light along their axis towards extraction at the top surface, as opposed to thin-films which are largely limited by total internal reflection[22]. However, when considering integration on Si, effects of the substrate need to be taken into account because the refractive index of Si is higher than GaN at most wavelengths in the visible spectrum. The potential for both increased IQE and light extraction from GaN nanowire-based LEDs on Si is an exciting prospect, and a comprehensive study of light extraction from such structures is essential for future large-scale integration. In this work, we use a combination of finite difference time domain (FDTD) photonic simulations and modal analysis to optimize extraction efficiency for emission from nonpolar GaN nanowires on Si with the final goal of designing optimized large scale arrays of GaN nanowire-based LEDs on Si.

## 2. METHODS

For this work, Lumerical FDTD Solutions was used to perform three-dimensional simulations of spontaneous emission from within a single GaN nanowire. A mode solver was used to solve for the dispersion of the guided modes within the nanowire, to excite emission modes within the nanowires for calculating the reflection coefficients of the modes, and to observe the longitudinal modes along the nanowire length.

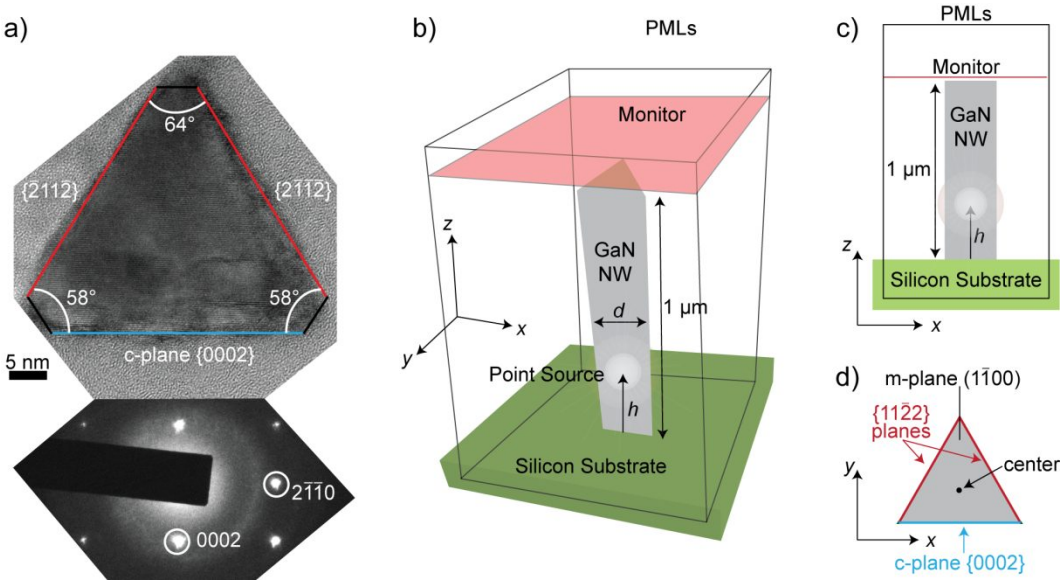


Figure 1. (a) Cross-sectional bright-field transmission electron microscope image of a MOCVD-grown *m*-directional GaN nanowire and the corresponding diffraction pattern. (b) Three-dimensional representation of the simulation volume used in this work. The dipole source is centered in the equilateral triangular cross-section of the nanowire and its height from the substrate, *h*, is varied. The power monitor immediately above the nanowire tip measures the effective extracted power, as more clearly shown in (c) the side view. (d) The nanowire cross-section, as estimated by an equilateral triangle, demonstrating the nanowire facets relative to the simulation axes.

The simulated nanowire structure is shown schematically in Figure 1. Our previous results have shown that a majority of MOCVD-grown GaN nanowires grow along the *m*-direction, regardless of the growth substrate[19,23]. Such *m*-directional GaN nanowires are defined by one polar $\{0002\}$ *c*-plane facet and two semi-polar $\{11\bar{2}2\}$ facets forming a triangular cross-section with two 58.4° angles and one 63.2° angle (Figure 1a). For simulation purposes, the *m*-directional GaN nanowire was approximated as a 1-μm long prism aligned vertically on the Si substrate and with an equilateral triangular cross-section of side-length *d* (Figure 1b-d). As a first approximation, the refractive index of the nanowire was set as $n = 2.6$ for all wavelengths of interest near the emission of GaN, and all reported values are for a wavelength of 381.15 nm, unless otherwise noted. The simulation boundaries were set to 400 nm away from the edges of the nanowire in the *x* and *y*-directions, about 600 nm above the nanowire tip and 500 nm below the nanowire-substrate interface in the *z*-direction.

The volume of the simulation was selected such that the measured extraction efficiencies did not change significantly when it was increased further, balancing calculation time and accuracy. At the edges of the simulation, a perfectly matched layer (PML) boundary condition was applied. The PMLs absorb any radiation that reaches the bounds of the simulation volume, effectively eliminating any reflection at the boundaries that could interfere with the simulation. The mesh applied in the region of the nanowire was chosen to be $d/50$ to best represent the diagonal sidewalls of the triangular cross-section with the rectangular mesh. At all other points in the simulation, the mesh step-size is approximately $\lambda/15n$. A power monitor was placed perpendicular to the substrate, directly above the tip of the nanowire to measure the extracted power.

To simulate incoherent spontaneous emission, as expected from LEDs, an electric dipole was used to simulate a recombination event within a QW. Generally, to simulate incoherent isotropic emission from a QW, a planar distribution of such point sources must be used and averaged over three orthogonal orientations[22]. For example, the general form of electric field intensity can be found by averaging the intensity from three separate simulations with a dipole source oriented in three orthogonal directions, as shown in Equation 1:

$$\left\langle \left|\vec{E}\right|^2 \right\rangle = \frac{1}{3}\left( \left|\vec{E}_x\right|^2 + \left|\vec{E}_y\right|^2 + \left|\vec{E}_z\right|^2 \right) \tag{1}$$

However, it has been shown that emission from *m*-directional InGaN QWs embedded in GaN is not isotropic[24]. The proportion of light intensities emitted from a thin-film was found to be approximately 90% and 10% for emission with the electric field perpendicular to the *c*-axis ($E\perp c$) and parallel to the *c*-axis ($E\parallel c$), respectively. The polarization preference arises from the band-structure, where there is an energy offset of ~49 meV between transitions for which $E\perp c$ and $E\parallel c$, such that the probability of a transition with $E\perp c$ is more favorable[24]. Assuming that the power emitted by each transition in nanowires is approximately equal to that in the thin-film case, the power average was calculated such that the *x* and *z*-oriented dipoles ($E\perp c$) were weighted by 0.9 and the *y*-oriented dipole ($E\parallel c$) was weighted by 0.1, with the direction defined as in Figure 1. The source was then placed in the cross-sectional center of the nanowire at varying distance from the substrate (denoted as *h* in Figure 1). We note that to more accurately assess the extraction efficiencies of axial heterostructures, multiple point sources within the *x*-*y* plane should be used; however, to reduce computational intensity, in this study point sources in the cross-sectional center of the nanowire were used.

The mode solver was used to calculate the dispersion of the modes existing in a nanowire waveguide by solving for the effective index of all confined modes near the GaN emission wavelength for nanowires with 100 nm ≤ $d$ ≤ 300 nm. To study the longitudinal modes within nanowires of various dimensions, a modal excitation source was used at the base of the nanowire for each mode. The steady-state intensity profile, $|E(z)|^2$, was then taken as the longitudinal mode corresponding to the mode used for excitation. The reflectivity at Si and air was calculated for each mode using the directional modal excitation source and a power monitor behind the source. For the reflection simulations, the nanowire was semi-infinite (achieved by setting up the nanowire beyond the PML in one direction) and encountered an interface at only one end to avoid measuring multiple reflections[25]. It should be noted that MOCVD-grown nanowires are typically grown using a metal seed-particle to template the one-dimensional growth as a preferential nucleation site, thus the nanowire tips are usually covered with this seed-particle. The simulations assume a flat facet at the tip, assuming the seed-particle has been removed, which can be achieved with a chemical etch[26].

## 3. RESULTS AND DISCUSSION

Figure 2 compares the extraction efficiency of GaN nanowires and that of a thin film as a function of the emission source position, *h* (see Figure 1). The extraction efficiency of a 1-μm thick *m*-directional film on Si is approximately 4% and relatively independent of *h*. In a simple structure similar to the thin-film structure simulated in this work, with just a GaN thin-film on a substrate, the light extraction has been experimentally shown to match these results, reported at 4%[27]. The two nanowires used in this study (unless otherwise noted) were selected to represent a waveguiding and non-waveguiding nanowire, with $d$ = 300 nm and $d$ = 60 nm, respectively. In the case of the waveguiding nanowire the electric field is mostly confined within the dimensions of the nanowire, while the non-waveguiding nanowire is below the cut-off for confining any modes. Extraction efficiencies of both the waveguiding and non-waveguiding nanowires are

generally higher than the extraction efficiency of the thin-film and dependent on the dipole source position (Figure 2). The relatively low thin-film extraction efficiency is caused by the low acceptance angle of light extracted from the thin-film (~22°) due to the high refractive index contrast between GaN and air. Thin-film extraction efficiencies can be greatly enhanced with further processing such as surface roughening, refractive index grading, photonic crystals and flip-chip designs with back-side reflectors and optimization of cavity dependent radiation, reaching extraction efficiencies up to 80%[28]. In contrast to thin-films, Figure 2 shows that simply by optimizing placement of the emission source in the nanowire, without any further processing steps, the extraction efficiency in nanowires can reach 50%.

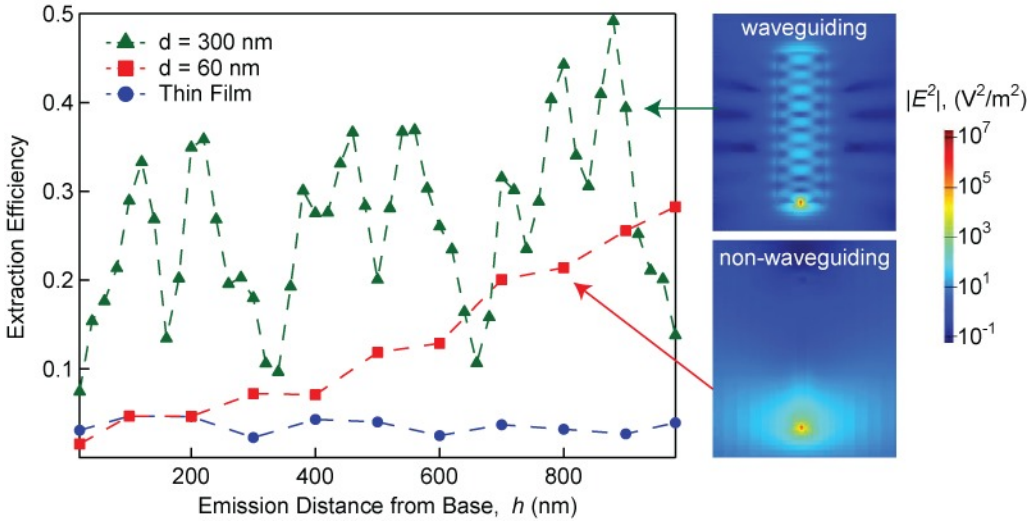


Figure 2. The extraction efficiency as a function of the emission distance from base, $h$, for a waveguiding nanowire ($d$ = 300 nm), a non-waveguiding nanowire ($d$ = 60 nm) and a thin-film of GaN, with electric-field intensity profiles (log-scale) of the nanowires shown on the right.

Though the nanowires have higher extraction efficiencies than the thin-film, they display very different dependencies on $h$ (Figure 2); for the waveguiding nanowires, most of the electric-field intensity is confined within the nanowire, but for much thinner nanowires (*e.g.* $d$ = 60 nm), the emission profile is similar to the case of a dipole in free-space above the substrate (with no nanowire present). Thus, the difference in extraction as a function of the dipole position is associated with the difference in nanowire waveguiding properties. In the non-waveguiding case, extraction efficiency increases steadily for increasing values of $h$, which can be attributed to an increasing angle of the downward-emitted light that is reflected at the Si-air interface. We note that for the simulation volumes used here, the maximum angle accepted as extracted via back-reflection from Si is approximately 18° from the substrate normal. Therefore, the reported extraction efficiencies are underestimated for cases where back-reflection from the Si is a significant portion of light extracted (as is the case for non-waveguiding nanowires) and the extraction efficiencies for the non-waveguiding nanowire are likely higher than we report. There is also a small periodic fluctuation of the extraction efficiency with $h$ for the non-waveguiding nanowire and the thin-film, likely due to cavity dependent radiation[28]. In the waveguiding nanowire, extraction efficiency is not a smooth function, but strong variations are observed as a function of $h$, which we next show is primarily due to changes in coupling of the point source emission into different modes as the emission source is moved axially along the wire.

To fully understand the dependency of extraction on $h$ in the waveguiding nanowire, we next investigated the modal dispersion. The dispersion of the first transverse electric (TE) and magnetic (TM) modes has previously been reported in the context of non-polar GaN nanowires for laser applications[29]. In this work, we calculate the dispersion of the first six modes, including the fundamental, TE and TM as well as higher order modes. Figure 3a shows the dispersion relation for the modes plotted with the size-normalized propagation constant, $\omega d/c$, as a function of the effective index, $n_{eff}$, where the mode is considered guided if $n_{eff} > 1$. The cross-sectional electric-field intensity profiles of the modes are also shown in Figure 3b. Nanowires with triangular cross-sections are single-mode waveguides, guiding only the fundamental mode, $HE_{11}$, from approximately $1.5 < \omega d/c < 2.5$ (corresponding to 95 nm < $d$ < 150 nm for $\lambda$ = 381 nm). In addition to $HE_{11}$, the $TM_{01}$ and $TE_{01}$ modes are guided at $\omega d/c$ above 2.5 and 3.2, respectively (corresponding to $d \geq 150$ nm and $d \geq 195$

nm, respectively, near $\lambda$ = 381 nm). Finally, at even larger $\omega d/c$, the higher order hybrid modes begin to be guided. Waveguide cross-sections that are not radially symmetric lift the degeneracy of the intensity profile of the modes, which are well known for a circular cross-section; hence the fundamental modes are $HE_{11}^{x}$ and $HE_{11}^{y}$ rather than simply $HE_{11}$, however these modes remain degenerate in terms of their properties (dispersion and reflection). Notably, even with reduced cross-sectional symmetry of the triangular nanowire, these modes have electric-field intensity profiles which are comparable to nanowires of hexagonal and circular cross-sections[22], however the difference between cross-sectional profiles of triangular and hexagonal nanowires is more notable in the higher order hybrid modes[30]. Thus for the lower order modes, it is likely that our results would hold for a properly normalized nanowire with a hexagonal cross-section[22].

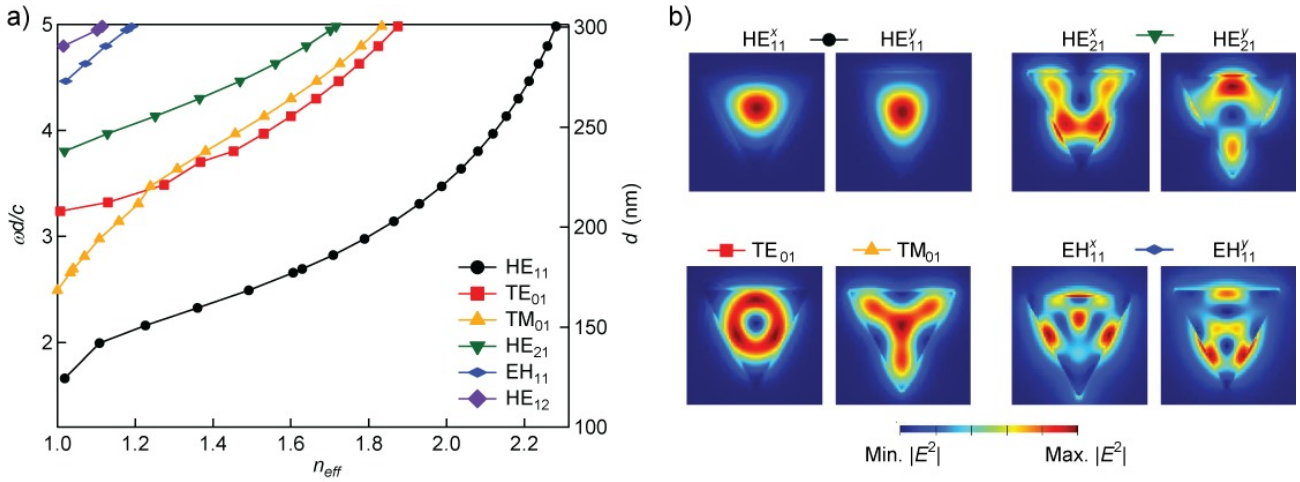


Figure 3. (a) Dispersion relation of the first six modes present in a triangular nanowire waveguide of GaN in air as calculated with a mode solver, with $d$ reported at $\lambda$ = 381 nm. (b) The cross-sectional electric-field intensity profile of the modes displayed above.

To elucidate the oscillatory-like dependency of extraction efficiency as a function of emission source distance from the substrate in the waveguided nanowire, it must be considered that the guided modes excite distinct longitudinal modes (electric-field intensity profile in the steady state) along the length of the nanowire. The longitudinal modes are independent of the modal excitation source placement, suggesting that the coupling of radiation from an incoherent emission source into a given mode depends on the magnitude of the corresponding mode's longitudinal electric-field intensity profile. For example, a dipole positioned at the maximum/minimum of a longitudinal electric-field intensity profile is expected to have strong/weak coupling into the corresponding mode. Although this principle accounts for the overall coupling into waveguided modes, the total extraction efficiency also depends on the reflection of each mode at the nanowire-air and nanowire-substrate interfaces, as we discuss next.

For high extraction efficiency, it is desirable to have high reflectivity at the nanowire-substrate interface, promoting back-reflection of the guided modes towards extraction, and a low reflectivity at the nanowire-air interface, where light is extracted. These considerations can be condensed to a ratio of the reflectivity at the substrate ($R_{Si}$) to reflectivity at the nanowire-air interface ($R_{Air}$), denoted here as $R_{Si}/R_{Air}$. We calculated both $R_{Air}$ and $R_{Si}$ as a function of $\omega d/c$ (Figure 4a and b, respectively). As expected, for a given mode, $R_{Air}$ approaches zero near the $\omega d/c$ for which that mode is near the waveguiding cutoff, because $n_{eff}$ is lower in this regime (Figure 2); the electric-field is less-confined within the nanowire and thus less of the radiation is incident upon the nanowire-air interface, leading to smaller $R_{Air}$. In contrast, each mode has a maximum $R_{Si}$ near the waveguiding cutoff. In this regime the electric-field intensity is less-confined within the nanowire and thus more of the radiation is outside the nanowire, which encounters the higher index-contrasted Si-air interface. As $\omega d/c$ increases, $n_{eff}$ increases such that the electric-field intensity of the mode is mostly confined within the nanowire and thus $R_{Si}$ approaches a constant value. Figure 4c demonstrates that the highest $R_{Si}/R_{Air}$ is achieved in the single mode region, where only the fundamental mode exists, at $\omega d/c$ = 1.6 (corresponding to $d$ = 105 nm for $\lambda$ = 381 nm). For the waveguiding nanowire, for which $\omega d/c \approx 5$ at $\lambda$ = 381 nm, $R_{Si}/R_{Air} < 1$ for every mode except the highest order hybrid mode, $HE_{12}$, meaning that coupling to these modes is unfavorable for extraction, since more radiation is guided into the Si substrate, where it is absorbed.

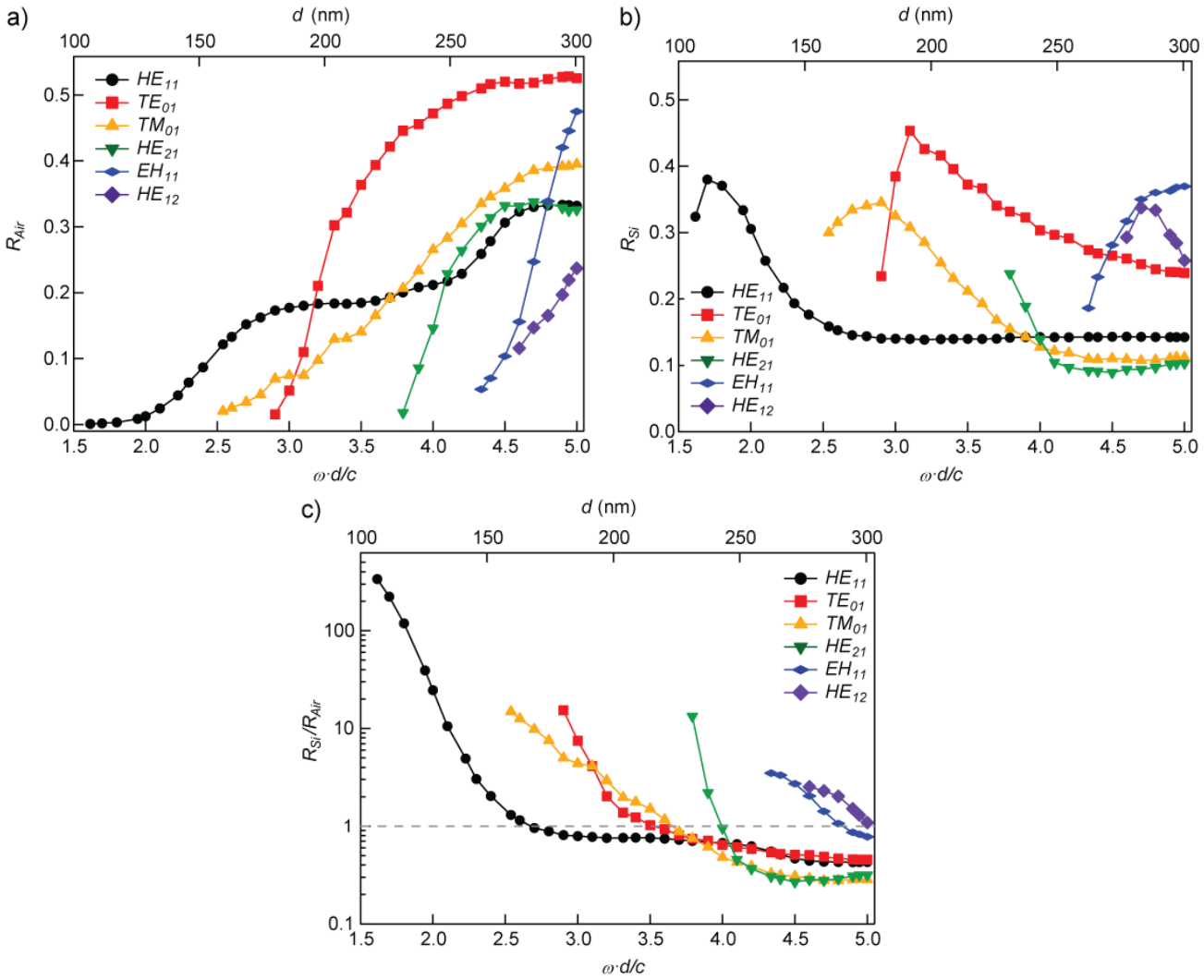


Figure 4. Waveguided mode reflectivity at the air interface - $R_{Air}$ (a), the substrate interface - $R_{Si}$ (b), and their ratio – $R_{Si}/R_{Air}$ (c), where the dashed line indicates $R_{Si}/R_{Air} = 1$, above which emission coupling into a mode enhances extraction, with all $d$ reported at $\lambda = 381$ nm.

To explain the dependency of extraction efficiency on $h$ for the waveguiding nanowire, we developed a simple model that incorporates coupling of the emission source into waveguided modes and $R_{Si}/R_{Air}$. Figure 5 shows the electric-field intensity of the longitudinal modes above the extraction efficiency for the waveguiding nanowire. Notably, the extraction efficiency maxima correspond to minima in the longitudinal profile of the fundamental mode, demonstrating that the extraction efficiency is high when coupling to the fundamental mode is expected to be low. For the waveguiding nanowire, $R_{Si}/R_{Air} = 0.42$ for the fundamental mode, indicating that any radiation coupled into the fundamental mode is guided into the substrate rather than out of the nanowire tip. A simple model was developed based on this concept, where extraction efficiency ($c_{ext}$) was calculated using Equation 2:

$$c_{ext} = \sum_m a_m \cdot I_m(h) \cdot \left( \frac{R_{Si}}{R_{Air}} - 1 \right)_m \tag{2}$$

Here, $a_m$ is the coupling coefficient to the mode $m$ and $I_m(h)$ is the longitudinal electric-field intensity profile. Using this model, we show that it accounts for the periodicity and most of the maxima and minima observed in the extraction efficiency for the waveguiding nanowire (Figure 5). The coupling coefficients calculated from the fit indicate low

coupling to modes with an antinode at the center of the electric-field intensity profile such as $TE_{01}$ (Figure 3b). The low coupling corresponds to the fact that the simulations were run with the emission source at the center of the nanowire, where it should have low coupling to modes with a minimum electric-field intensity at the center of the nanowire. This fact emphasizes the need for planar source simulations, because in full axial heterostructures, coupling to these modes would be expected to be higher. To further verify that the extraction efficiency is dependent on coupling along the length of the nanowire, we consider a single-mode nanowire with $d$ = 105 nm, near the maximum $R_{Si}/R_{Air}$ found (Figure 4c). In this case the fundamental mode is the only mode guided at $\lambda$ = 381 nm (Figure 6), demonstrating that the coupling of the emission source into the waveguided mode is the dominant consideration for light extraction, as the electric-field intensity of the fundamental mode and the extraction efficiency as a function of $h$ are nearly identical in periodicity.

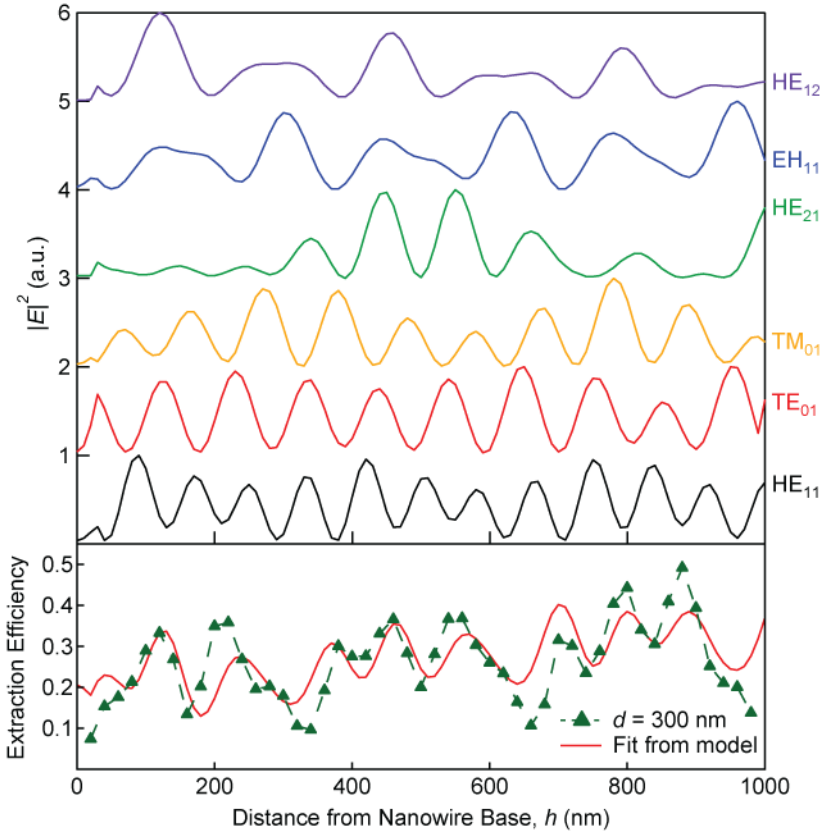


Figure 5. The longitudinal profile of the waveguided modes in a nanowire ($d$ = 300 nm) as compared with extraction efficiency. The solid line is the calculated fit of the model, which incorporates coupling to these modes and their reflection at the interfaces.

This work has developed a simple route to predict the optimal placement of a point source for extraction, but further work is ongoing that includes a confinement factor for radiation within the nanowire waveguide, because though weakly confined modes may have the highest $R_{Si}/R_{Air}$, it is possible that the extraction efficiency could be higher for more confined modes, where weakly confined modes have a substantial amount of radiation in the $x$ and $y$ directions. As mentioned above, it will also be important to simulate full planar sources. Furthermore, it is of interest to apply a similar approach at other wavelengths, specifically for red, green and blue emission. Finally, to understand the full potential of GaN nanowire-based LEDs, these simulations will be scaled up to include arrays of nanowires, which may be able to enhance extraction by scattering emission up to be collected or potentially by arranging the nanowires to form a photonic crystal to encourage vertical light propagation only.

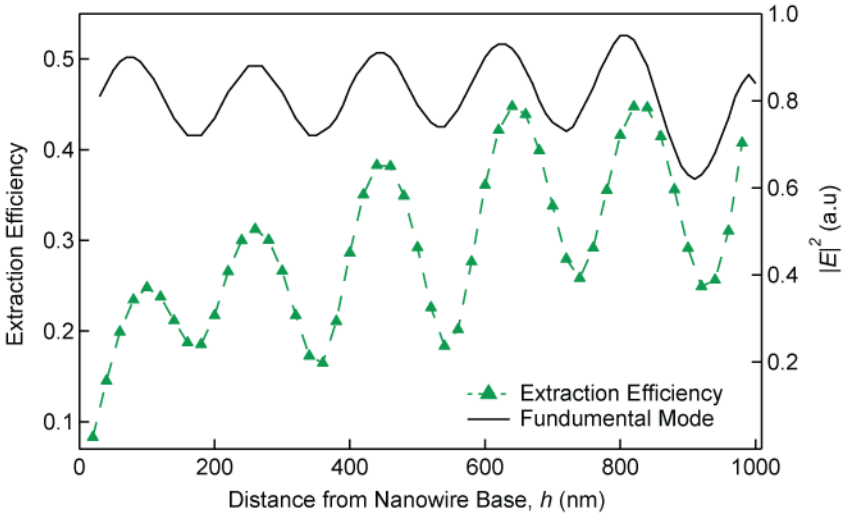


Figure 6. The extraction efficiency as a function of $h$ as compared to the longitudinal profile in a nanowire with $d$ = 105 nm, where only the fundamental mode exists.

## 4. CONCLUSIONS

In conclusion, GaN nanowires grown on Si provide a uniquely advantageous platform towards solid state lighting. Specifically, in *m*-directional GaN nanowires it may be possible to increase both the IQE and extraction efficiency compared to simple thin-film devices. We demonstrated that both waveguiding and non-waveguiding nanowires can show improved extraction over thin-film devices. For waveguiding nanowires, we have determined the extraction efficiency as a function of the emission source placement along the nanowire length, by using FDTD to consider electric-field intensity longitudinal modes and reflection at the interfaces. These results suggest a general method to optimizing the placement of a QW within axial heterostructure GaN-based nanowire LEDs, however further work is needed to more accurately represent axial heterostructures. Work is ongoing to expand these results using full planar sources and investigate wavelengths in the visible spectrum. By improving nanowire-based LED design for light extraction on a scalable Si platform, these results will be able to guide experimental work in fabricating highly efficient nanowire-based LEDs.

## REFERENCES

[1] Humphreys, C.J., "Solid State Lighting," MRS Bulletin 33, 459-470 (2008).

[2] Kasap, S., and Capper, P., [Group III Nitrides], Springer Handbook of Electronic and Photonic Materials, 753-804 (2007).

[3] Komissarova, T. A., Jmerik, V.N., Mizerov, A.M., Shmidt, N.M., Ber, B.Y., Kasantsev, D.Y., and Ivanov, S.V., "Electrical properties of Mg-doped GaN and AlxGa1-xN," Physica Status Solidi (C) 6(S2), S466-S469 (2009).

[4] Zhihao, X., Jincheng, Z., Huantao, D., Zhongfen, Z., Qingwei, Z., Hao, X., and Yue, H., "Stress, structural and electrical properties of Si-doped GaN film grown by MOCVD," Journal of Semiconductors 30(12), 123003 (2009).

[5] Pearton, S.J., Ren, F., Zhang, A.P., Dang, G., Cao, X.A., Lee, K.P., Cho, H., Gila, B.P., Johnson, J.W., et al., "GaN electronics for high power, high temperature applications," Materials Science and Engineering: B 82(1-3), 227-231 (2001).

[6] Palacios, T., Chakraborty, A., Heikman, S., Keller, S., Denbaars, S.P., and Mishra, U.K., "AlGaN / GaN High Electron Mobility Transistors With InGaN Back-Barriers," IEEE Electron Device Letters 27(1), 2005-2007 (2006).
[7] Azize, M., Hsu, A.L., Saadat, O.I., Smith, M., Gao, X., and Guo, S., "High-Electron-Mobility Transistors Based on InAlN / GaN Nanoribbons," IEEE Electron Device Letters 32(12), 1680-1682 (2011).
[8] Paszkiewicz, R., Paszkiewicz, B., Wosko, M., Szyszka, a., Marciniak, L., Prażmowska, J., Macherzyński, W., Serafińczuk, J., Kozłowski, J., et al., "Properties of MOVPE GaN grown on ZnO deposited on Si(001) and Si(111) substrates," Journal of Crystal Growth 310(23), 4891-4895 (2008).
[9] Radtke, G., Couillard, M., Botton, G. a., Zhu, D., and Humphreys, C.J., "Structure and chemistry of the Si(111)/AlN interface," Applied Physics Letters 100(1), 011910 (2012).
[10] Krost, A., and Dadgar, A., "Heteroepitaxy of GaN," in 12th International Conference on Semiconducting and Insulating Materials, 41-47 (2002).
[11] Schubert, E.F., [Light-Emitting Diodes], Second Edition, Cambridge University Press, Cambridge, UK (2006).
[12] Jellison, G.E., "Optical constants for silicon at 300 and 10 K determined from 1.64 to 4.73 eV by ellipsometry," Journal of Applied Physics 53(5), 3745 (1982).
[13] Chang, S.J., Chang, C.S., Su, Y.K., Lee, C.T., Chen, W.S., Shen, C.F., Hsu, Y.P., Shei, S.C., and Lo, H.M., "Nitride-Based Flip-Chip ITO LEDs," IEEE Transactions on Advanced Packaging 28(2), 273-277 (2005).
[14] Baron, N., Cordier, Y., Chenot, S., Vennéguès, P., Tottereau, O., Leroux, M., Semond, F., and Massies, J., "The critical role of growth temperature on the structural and electrical properties of AlGaN/GaN high electron mobility transistor heterostructures grown on Si(111)," Journal of Applied Physics 105(3), 033701 (2009).
[15] Qian, F., Gradečak, S., Li, Y., Wen, C.-Y., and Lieber, C.M., "Core/multishell nanowire heterostructures as multicolor, high-efficiency light-emitting diodes," Nano Letters 5, 2287-2291 (2005).
[16] Zhong, Z., Qian, F., Wang, D., and Lieber, C.M., "Synthesis of p-Type Gallium Nitride Nanowires for Electronic and Photonic Nanodevices," Nano Letters 3(3), 343-346 (2003).
[17] Tang, Y.B., Chen, Z.H., Song, H.S., Lee, C.S., Cong, H.T., Cheng, H.M., Zhang, W.J., Bello, I., and Lee, S.T., "Vertically aligned p-type single-crystalline GaN nanorod arrays on n-type Si for heterojunction photovoltaic cells.," Nano letters 8(12), 4191-5 (2008).
[18] Guo, W., Banerjee, A., Bhattacharya, P., and Ooi, B.S., "InGaN/GaN disk-in-nanowire white light emitting diodes on (001) silicon," Applied Physics Letters 98(19), 193102 (2011).
[19] Zhou, X., Chesin, J., Crawford, S., and Gradečak, S., "Using seed particle composition to control structural and optical properties of GaN nanowires.," Nanotechnology 23(28), 285603 (2012).
[20] Lim, S.K., Crawford, S., Haberfehlner, G., and Gradečak, S., "Controlled Modulation of Diameter and Composition along," Nano Letters ASAP, 18-23 (2012).
[21] Ni, X., Lee, J., Wu, M., Li, X., Shimada, R., Özgür, U., Baski, a. a., Morkoç, H., Paskova, T., et al., "Internal quantum efficiency of c-plane InGaN and m-plane InGaN on Si and GaN," Applied Physics Letters 95(10), 101106 (2009).
[22] Henneghien, A.-L., Gayral, B., Désières, Y., and Gérard, J.-M., "Simulation of waveguiding and emitting properties of semiconductor nanowires with hexagonal or circular sections," Journal of the Optical Society of America B 26(12), 2396 (2009).
[23] Lim, S.K., Crawford, S., and Gradečak, S., "Growth mechanism of GaN nanowires: preferred nucleation site and effect of hydrogen.," Nanotechnology 21(34), 345604 (2010).
[24] Gardner, N.F., Kim, J.C., Wierer, J.J., Shen, Y.C., and Krames, M.R., "Polarization anisotropy in the electroluminescence of m-plane InGaN–GaN multiple-quantum-well light-emitting diodes," Applied Physics Letters 86(11), 111101 (2005).

[25] Maslov, a. V., and Ning, C.Z., "Reflection of guided modes in a semiconductor nanowire laser," Applied Physics Letters 83(6), 1237 (2003).
[26] Tambe, M.J., Ren, S., and Gradečak, S., "Effects of Gold Diffusion on n-Type Doping of GaAs Nanowires.," Nano letters 10(11), 4584-4589 (2010).
[27] Kumnorkaew, P., Gilchrist, J.F., and Tansu, N., "Light Extraction Efficiency and Radiation Patterns of III-Nitride Light-Emitting Diodes With Colloidal Microlens Arrays With Various Aspect Ratios," IEEE Photonics Journal 3(3), 489-499 (2011).
[28] Krames, M.R., Shchekin, O.B., Mueller-Mach, R., Mueller, G.O., Zhou, L., Harbers, G., and Craford, M.G., "Status and Future of High-Power Light-Emitting Diodes for Solid-State Lighting," Journal of Display Technology 3(2), 160-175 (2007).
[29] Seo, M.-K., Yang, J.-K., Jeong, K.-Y., Park, H.-G., Qian, F., Ee, H.-S., No, Y.-S., and Leet, Y.-H., "Modal characteristics in a single-nanowire cavity with a triangular cross section.," Nano Letters 8(12), 4534-8 (2008).
[30] Vassallo, C., [Optical Waveguide Concepts], First Edition, Elsevier Science Publishing Company, Inc., New York, NY, 61-67 (1991).